ISSN 1990-7931, Russian Journal of Physical Chemistry B, 2016, Vol. 10, No. 4, pp. 621–627. © Pleiades Publishing, Ltd., 2016.
Original Russian Text © B.P. Aduev, N.R. Nurmukhametov, R.P. Kolmykov, A.P. Nikitin, M.V. Anan'eva, A.A. Zvekov, A.V. Kalenskii, 2016, published in Khimicheskaya Fizika, 2016, Vol. 35, No. 8, pp. 37–43.

COMBUSTION, EXPLOSION, AND SHOCK WAVES

Explosive Decomposition of Pentaerythritol Tetranitrate Pellets Containing Nickel Nanoparticles with Various Radii

B. P. Aduev[a], N. R. Nurmukhametov[a], R. P. Kolmykov[b], A. P. Nikitin[a], M. V. Anan'eva[b, *], A. A. Zvekov[a], and A. V. Kalenskii[b, *]

[a] *Institute of Coal Chemistry and Material Science, Siberian Branch, Russian Academy of Sciences, Kemerovo, 650000 Russia*
[b] *Kemerovo State University, Kemerovo, 650043 Russia*
**e-mail: kriger@kemsu.ru*

Received June 1, 2015

Abstract—The kinetics of the explosive decomposition of pressed pentaerythritol tetranitrate pellets containing nickel nanoparticles with various radii has been investigated experimentally, with the explosion initiated by a neodymium laser pulse (wavelength, 1064 nm; pulse duration at half-height, 14 ns), and probability curves for this process have been recorded. The experimental values of critical initiation energy density corresponding to 50% explosion probability are 0.9, 0.7, and 1.4 J/cm^2 at a nickel particle radius of 67, 78, and 138 nm, respectively. The initial time interval in which the intensity of light emission accompanying the explosive decomposition increases begins during the action of the pulse and is described by a Gaussian function with an effective constant of $k = (1.4 \pm 0.1) \times 10^8$ s^{-1}, which is independent of the nanoparticle radius. Experimental data of this study can be interpreted within the micro-hotspot model of thermal explosion.

Keywords: laser initiation, explosive decomposition, energetic materials, pentaerythritol tetranitrate, nickel nanoparticles, mathematical modeling

DOI: 10.1134/S1990793116040187

INTRODUCTION

The safety of blasting operations in the mining industry can be enhanced by using optical detonators. This approach that was suggested earlier [1, 2] and is now being actively developed. The greatest effect of employing optical detonators can be attained with energetic materials that are selectively sensible to laser radiation and have relatively high initiation thresholds for other initiation types (shock, electric spark, heating, etc.). The problem of developing energetic materials that are selectively sensible to laser radiation is addressed by synthesizing novel explosives, including metal–tetrazole derivative complexes [3–5]. An alternative approach is introducing light-absorbing particles into the existing explosives [6–8]. In earlier studies [9–11], we experimentally determined the initiation threshold for the explosive decomposition of pentaerythritol tetranitrate (PETN) containing aluminum nanoparticles. It was demonstrated that this material is sensible to laser radiation at the 1 J/cm^2 level, which is two orders of magnitude lower than in the case of pure pressed PETN pellets [12], for which the critical initiation energy density is at least 100 J/cm^2 (while the shock initiation threshold is unaffected by aluminum nanoparticles). It was investigated how the laser initiation threshold depends on the nature of the metal and radiation wavelength [9, 10]. There have been studies on the optical properties of pressed PETN–aluminum [13, 14], PETN–cobalt [15], and PETN–nickel [16] pellets and on the kinetics of the explosive luminescence of pressed PETN–aluminum pellets under laser initiation conditions was [11].

In order to explain the regularities of the laser initiation of secondary explosives containing metal nanoparticles, we modified the micro-hotspot model [17, 18], which was initially formulated for the initiation of heavy-metal azides [19, 20]. It was demonstrated that promising admixtures are iron-subgroup metal particles with a radius of about 100 nm [17]. One of the most important corollaries of the model is that the critical initiation energy density as a function of the radius of the nanoparticles introduced passes through an extremum [17]. Here, we report the explosive decomposition kinetics and critical initiation energy density for pressed PETN pellets containing nickel nanoparticles of various sizes and compare the experimental data with the results of mathematical modeling.

EXPERIMENTAL

The experimental setup used in this work was reported earlier [9–11]. The source of pulsed radiation was a Nd : YAG laser operating in the Q-switching mode. The pulse duration was 14 ns, the maximum

pulse energy at the fundamental frequency was 1.54 J, and the wavelength was 1064 nm. A beam with a uniform illuminance distribution and sharp contrast at its boundaries was formed by the projection method, which provides means to record light emission solely from the sample area irradiated by the laser beam [21]. The method of detecting light emission from the irradiated area of a sample was suggested for, and tested in, kinetic studies of the explosive decomposition of primary explosives, and it made it possible to separate the onset and development of the reaction and the expansion of explosion products [22]. In this work, this method was used to study the explosive decomposition of pressed PETN–nickel pellets.

The kinetics of light emission resulting from explosive decomposition was studied using a panoramic photomultiplier, which registered light emission from the entire cell volume, and a photomultiplier that registered light emission from the irradiated area [23]. The experimental samples were pressed PETN pellets containing 0.1 wt % nickel nanoparticles. (The samples containing 0.1 wt % nanoparticles are characterized by the lowest critical initiation energy density [9–11]. A PETN powder with a particle size distribution maximum at 1–2 μm was mechanically mixed with a nickel powder. The mixture was homogenized in an ultrasonic bath to obtain a uniform distribution of nickel particles throughout the mixture volume. Samples were pressed for 30 min at a maximum pressure of 1.8 GPa using a hydraulic press. The die was a 1-mm-thick copper plate with a hole 3 mm in diameter at its center [9–11]. The pellets obtained in this way were 3 mm in diameter and 1 mm in thickness and had a mass of (12.2 ± 0.2) mg and a density of (1.73 ± 0.03) g/cm^3.

Nanosized nickel particles were prepared by reducing an aqueous solution of nickel chloride with hydrazine hydrate [24]. The reaction was carried out in a Readleys chemical reactor fitted with a Lauda ECO E4 thermostat and a Heidolph RZR 2102 Control mechanical stirrer with a centrifugal impeller. This reactor provides means to precisely regulate the reaction temperature and stirring intensity, ensuring control over the synthesis parameters. Varying the reaction conditions made it possible to obtain metal nanoparticles of different sizes [24]. Experimental samples were prepared using nickel powders obtained under three different sets of conditions. The nanoparticles had a near-spherical shape, and their radius (R) at the size distribution maximum was 67, 78, and 138 nm, respectively. The variances of the particle size distributions (δR data) are listed in the table.

RESULTS

In order to determine the critical energy density for explosion initiation, we carried out tests at fixed values of laser pulse energy density and determined the probability of an explosion taking place. Next (as in our previous studies [9–11, 25, 26]), we plotted the explosion probability as a function of the pulse energy density (explosion probability curve). The critical energy density was taken to be the value corresponding to 50% explosion probability.

Figure 1 plots the observed probability of the explosion of PETN–nickel pellets (p) as a function of laser pulse energy density (H). The curves indicate an energy density region in which an explosion is not initiated. This region is followed by an H interval in which the explosion probability increases from 0 to 1. These probability curves are similar to those observed for PETN [9–11, 26] and primary explosives [25], but they differ in critical energy density and variance from the latter. The $p(H)$ curves were fitted to the integral error function

$$p = \frac{1}{\sqrt{2\pi}\sigma}\int_0^H \exp\left[-\frac{(H - H_c)^2}{2\sigma^2}\right]dH, \qquad (1)$$

where H_c is the critical energy density and σ is variance. The parameters of the explosion probability curves are listed in the table. It follows from these data that the critical initiation energy density takes the smallest value for nickel particles 78 nm in radius (Fig. 1, curve *2*). The table includes the critical energy densities normalized to the H_c value for a particle radius of 78 nm, $X^{\exp} = H_c^{\exp}(R)\big/H_c^{\exp}(R = 78\text{ nm})$. For the particles having a larger radius (138 nm) or a smaller radius (67 nm), the critical energy density is, respectively, 2 and 1.3 times higher than for the $R = 78$ nm particles.

Prior to investigating the kinetics of the explosive decomposition of the samples, we illuminated the photographic film to determine the photomultiplier signal synchronization time [11]. In case there were variations in the synchronization time and in the amplitudes of signals at their front, we minimized the sum of the squared deviations for the photomultiplier and laser pulse signals. The absorption of a laser pulse gave rise to light emission, which was detected by the zonal and panoramic photomultipliers. The observed synchronization time was 12 and 16 ns for the zonal and panoramic photomultipliers, respectively. The time dependence of the power of the laser pulse incident on a nickel nanoparticle with a radius R, $J(t)$, is similar to the Gaussian function [27]. Setting the initial point in time to be the position of the pulse maximum, we obtain the following relationship:

$$J(t) = \sqrt{\pi}k_i R^2 H \exp\left(-k_i^2 t^2\right), \qquad (2)$$

where k_i is the parameter characterizing the pulse duration at half-height.

Irradiation of a PETN–nickel pellet with a pulse whose power is insufficient for the initiation of explosive decomposition causes cracking of the sample and an outburst of part of its matter, forming a cavity. Figure 2 shows a typical oscillogram of light emission under subthreshold conditions. The signals from the zonal

and panoramic photomultipliers are separated by the synchronization time. The curves have one maximum; the frontal sides of all of the three curves coincide, and, therefore, the light emission intensity is proportional to the absorbed pulse intensity. The effective rate constants of the increase in the intensity of the photomultiplier signals and laser pulse, as calculated using the error function approximation, are similar and are $k_i = (1.2 \pm 0.2) \times 10^8$ s^{-1}. On the tail side of the peak, the intensity of light emission from the irradiated area decreases at a lower rate than the intensity of light emission from the entire cell.

We measured kinetic characteristics of light emission accompanying the explosive decomposition of pressed PETN–nickel pellets under the action of a laser pulse with an overcritical energy density. The explosion is accompanied by a loud sound and by an outburst of the entire energetic material pressed in the cooper plate. The initial increase in the light emission intensity measured by the zonal and panoramic photomultipliers (Fig. 3) is described by a Gaussian function with an effective constant of $k = (1.4 \pm 0.1) \times 10^8$ s^{-1}. The kinetics of light emission from the irradiated area shows two extrema; the first maximum almost coincides with the maximum of the laser pulse, while the second one is an extensive plateau up to 700 ns in length followed by a 200-ns-long decay. The maximum of light emission from the entire cell is observed earlier than the pulse intensity maximum. A specific kinetic feature of the explosive decomposition of the pressed PETN–nickel pellets is the absence of an induction period (time interval between the end of the pulse and the onset of intensive decomposition). Light emission (like radioluminescence) begins without any delay. The absence of an induction period is a feature differentiating thermal explosion from chain explosion: in the latter case, there is a distinct induction period after the end of the pulse [17].

MICRO-HOTSPOT MODEL OF THERMAL EXPLOSION

The micro-hotspot model is a variant of the thermal explosion model and is based on the assumption that, in the bulk of the transparent energetic material, there are inclusions that readily absorb laser radiation. The system of differential equations describing conductive heat transfer in a metal nanoparticle and in the exothermally decomposing surrounding matrix takes the following form for spherical symmetry [10, 11]:

$$\frac{\partial T}{\partial t} = \alpha\left(\frac{\partial^2 T}{\partial x^2} + \frac{2}{x}\frac{\partial T}{\partial x}\right) + \frac{Q}{c}k_0 n \exp\left(-\frac{E}{k_B T}\right), \quad x > R,$$
$$\frac{\partial n}{\partial t} = -k_0 n \exp\left(-\frac{E}{k_B T}\right), \quad x > R, \qquad (3)$$
$$\frac{\partial T}{\partial t} = \alpha_M\left(\frac{\partial^2 T}{\partial x^2} + \frac{2}{x}\frac{\partial T}{\partial x}\right), \quad x < R,$$

Parameters of the nickel nanoparticles and those of the probability curves for the explosive decomposition of PETN–nickel pellets

R, nm	δR, nm	H_c^{exp}, J/cm^2	X^{exp}	σ, J/cm^2	Q_{abs}	H_c^{th}, J/cm^2	X^{th}
67	3	0.9	1.3	0.1	0.7694	0.090	1.2
78	3	0.7	1.0	0.1	0.9544	0.074	1
138	7	1.4	2.0	0.2	0.8391	0.107	1.4

where T is temperature, n is the undecomposed fraction of the explosive (initial condition: $n = 1$), $\alpha = 1.1 \times 10^{-3}$ cm^2 s^{-1} and $\alpha_M = 0.23$ cm^2 s^{-1} are the thermal diffusivities of PETN and nickel, k_B is the Boltzmann constant, $E = 165$ kJ/(mol K) is the activation energy, $Q = 9.64$ kJ/cm^3 is the heat of decomposition, $k_0 = 1.2 \times 10^{16}$ s^{-1} [28] is the pre-exponential factor, and $c = 2.22$ J/(cm^3 K) is the volumetric heat capacity of PETN.

Spherical symmetry was accepted for the reason that laser light is multiply scattered by grain boundaries and metal nanoparticles. Because of the randomness of light reflection events, illuminance is averaged over all directions, so it is possible to use spherical symmetry in the calculations (as was done in earlier works [10, 11]).

At the nanoparticle–matrix boundary ($x = R$), light absorption takes place, implying the following boundary condition:

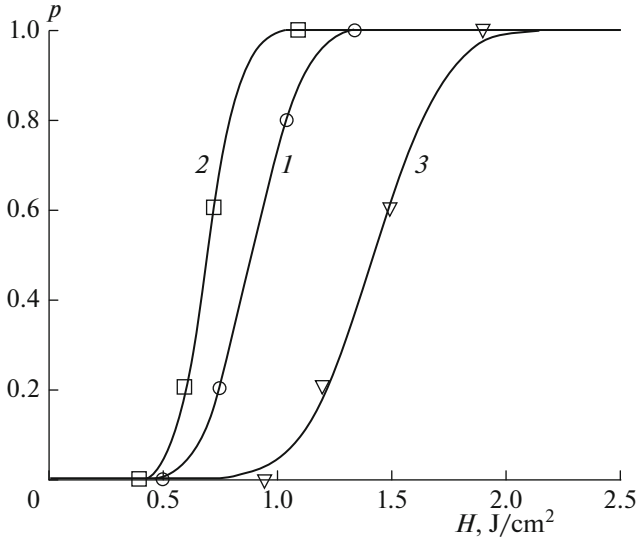

Fig. 1. Experimentally observed explosion probability p for PETN–nickel pellets as a function of the laser pulse energy H for nickel particles with a radius of (*1*) 67, (*2*) 78, and (*3*) 138 nm. The points represent experimental data, and the lines are fits to Eq. (1).

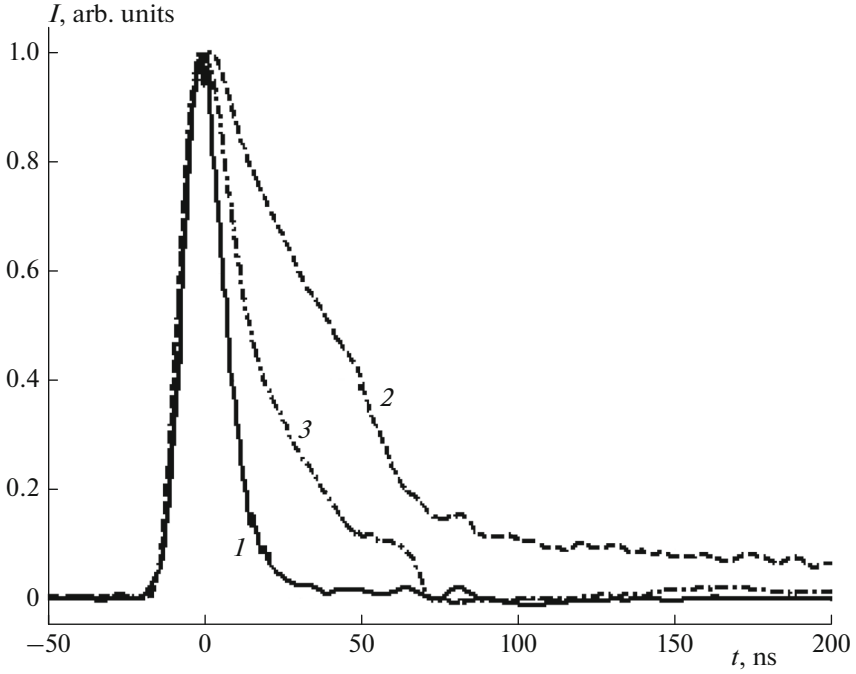

Fig. 2. Kinetics of light emission by PETN–nickel pellets under subthreshold conditions: (*1*) signal from the initiating pulse, (*2*) signal from the zonal photomultiplier, and (*3*) signal from the panoramic photomultiplier.

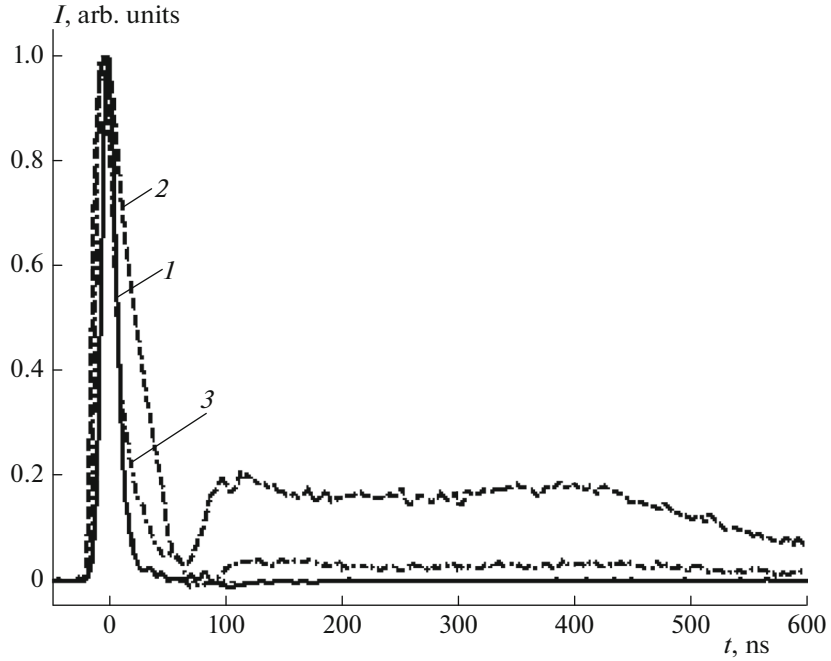

Fig. 3. Oscillograms of light emission from PETN–nickel pellets during their explosive decomposition: (*1*) initiating pulse, (*2*) zonal photomultiplier, and (*3*) panoramic photomultiplier.

$$\frac{Q_{\text{abs}}J}{4\pi R^2} - c_M\alpha_M\left.\frac{\partial T}{\partial x}\right|_{x\to R-0} + c\alpha\left.\frac{\partial T}{\partial x}\right|_{x\to R+0} = 0, \quad (4)$$

where $c_M = 3.96$ J/(cm^3 K) is the volumetric heat capacity of nickel and Q_{abs} is the laser radiation absorption efficiency [14–19].

The values of Q_{abs} were calculated within the Mie theory via the procedure described in our earlier works [13–17] for the complex refractive index of nickel at a wavelength of 1064 nm, which is $2.61-5.84i$ [29], and for the refractive index of the medium (PETN), which

is 1.54. At the boundary of the region examined (inclusion and an energetic material layer with a thickness of 7R), we accepted a Dirichlet boundary condition, namely, T = 300 K. The procedure of solving model equations (2)–(4) for calculating the critical and kinetic regularities of the explosive decomposition process was reported earlier [30].

Figure 4 plots the calculated dependences of the light absorption efficiency Q_{abs} (for a wavelength of 1064 nm) and the critical energy density for explosion initiation, H_c, on the radius of the nickel nanoparticles. It follows from these data that, in the particle radius range examined, Q_{abs} passes through a maximum at R = 96.1 nm, with Q_{abs} = 1.09 at this point. The critical energy density as a function of particle radius passes through a minimum at R = 90.9 nm. The lowest critical energy density in the radius range examined is 0.069 J/cm^2. Similar dependences were calculated for aluminum nanoparticles in the PETN matrix [10, 11]. The position of the maximum in the Q_{abs} versus R curve is close to the position of the minimum in the H_c versus R curve (96.1 and 90.9 nm, respectively), indicating that the optical properties of the nanoparticles play a dominant role under the given conditions. The calculated Q_{abs} and H_c values for the nanoparticles radii examined in the experiments are listed in the table. The critical energy density for the R = 67 and 138 nm nanoparticles is higher than the minimum H_c value, observed for R = 78 nm, by a factor of X^{th} = 1.2 and 1.4, respectively.

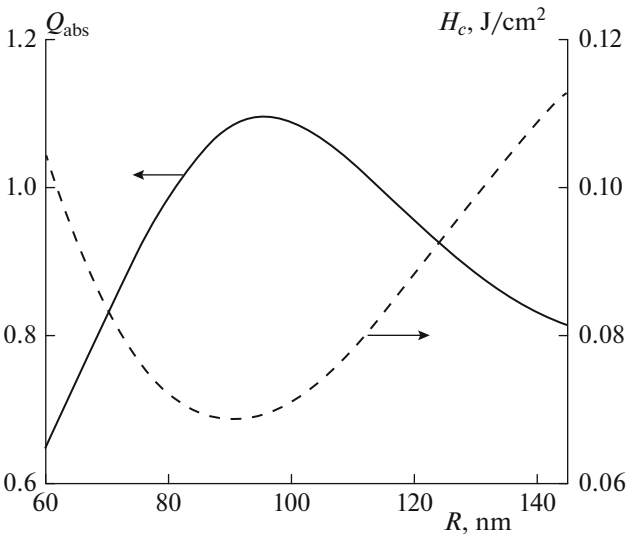

Fig. 4. Calculated light absorption efficiency (Q_{abs}) for the first harmonic of the neodymium laser (1064 nm) and critical energy density for the initiation of the explosive decomposition of the PETN–nickel composite (H_c) as a function of the nickel nanoparticle radius.

DISCUSSION

The measured critical energy density of the initiating laser pulse depends on the average size of the nickel nanoparticles admixed to the explosive (Fig. 1, table). A fundamental distinction here is that the lowest critical energy density is observed for an intermediate particle size and the critical energy density as a function of particle radius passes through an extremum. The particle size effect is pronounced fairly well: as the radius is changed by a factor smaller than 2, the critical energy density increases by 30–100%. This increase far exceeds the possible error of determination of critical energy density, which can be taken to be equal to σ (table). This information is necessary for optimizing explosive compositions for optical detonators, since particle size turned out to be a significant factor that can be tuned so as to substantially reduce the critical initiation energy density and to optimize the performance parameters of explosive devices.

Another issue to be considered is consistency between theory and experimental data. The critical energy density versus nanoparticle radius curve has a minimum point, whose existence is mainly due to the fact that the optical properties of the nanoparticles (light absorption efficiency) vary as their radius increases. This is indicated by the finding that the position of the maximum in the Q_{abs} versus R curve is close to the position of the minimum in the H_c versus R curve (Fig. 4). Theoretical calculations correctly reconstruct the observed tendency and the region in which the particle size effect shows itself. Therefore, the observed correlation can be considered as strong evidence in favor of the applicability of the microhotspot model of thermal explosion to the laser initiation of explosion in pressed pellets.

At the same time, there are two facts indicating that it is necessary to further develop the model: firstly, the experimental absolute values of critical energy density differ from theoretical ones; secondly, the nanoparticle radius effect predicted by the theory is less pronounced that the observed effect. The difference between the absolute values of critical energy density may arise from the fact that the model involves an insufficiently detailed conception of the mechanism of the decomposition reaction. The rate constants of the decomposition of explosives are typically measured at 350–450 K. A compensation effect appears in deriving the pre-exponential factor and activation energy from experimental data [31], and, because of this effect, these parameters may vary widely. In the extrapolation of rate constants to high temperatures at which the formation of an explosive decomposition spot takes place (~1000 K) [18], the error of determination of the rate constant of the rate-limiting step of the reaction will increase. In addition, it is necessary to take into account the temperature effect on the pre-exponential factor. Large values of the pre-exponential factor and,

accordingly, a high activation entropy for the breaking of molecules into radicals are known to be due to transition from hindered rotation in the ground state to the free rotation of the leaving group in the activated complex [32, 33]. As the temperature is raised, the effect of the potential barrier to hindered rotation decreases and so does the activation entropy. In the light of these considerations, it would be expected that the preexponential factor for free-radical abstraction reactions, to which the primary step of PETN decomposition belongs [27], will decrease with an increasing temperature. Another factor leading to a decrease in the effective rate constant is that the mechanism of the explosive decomposition reaction consists of a number of steps. With an increasing temperature, there can be a change of the rate-limiting step of the process and variations in effective Arrhenius parameters of the reaction.

A possible physical cause of the increase in the critical initiation energy density for the pressed pellets is the partial disintegration of the sample under the action of the laser pulse. Part of the pulse energy is spent on matter outburst and cavity formation. Taking these circumstances into consideration might ensure a better agreement between the theoretical and experimental absolute values of critical energy density.

CONCLUSIONS

Probability curves were obtained experimentally for the explosive decomposition of pressed PETN pellets containing nickel nanoparticles of various sizes upon initiation with nanosecond laser pulses. The critical initiation energy density was demonstrated to be a nonmonotonic function of the radius of the nickel nanoparticles. The critical energy density for the particle radii examined in the experiments was calculated within a modified micro-hotspot model of the laser initiation of explosion. The results of modeling are in agreement with the experimental data, but the model needs to be further refined. The results of this study are necessary for developing a procedure for optimizing explosive compositions to be used in optical detonators.

ACKNOWLEDGMENTS

The authors are very grateful to Prof. V.G. Kriger and Prof. V.P. Tsipilev for their interest in this study.

This study was supported by the Ministry of Education and Science of the Russian Federation (state assignment no. 3603, task 2014/64), by the Russian Foundation for Basic Research (grant no. 14-03-00534 A), and by grant no. MK-4331.2015.2 from the President of the Russian Federation.

REFERENCES

1. E. I. Aleksandrov and V. P. Tsipilev, Kvant. Electron. **7** (13), 79 (1980).
2. V. I. Tarzhanov, B. V. Litvinov, A. D. Zinchenko, N. P. Kozeruk, and V. I. Sdobnov, Izv. Vyssh. Uchebn. Zaved., Gorn. Zh., Nos. 9–10, 94 (1999).
3. S. C. Kunz and F. J. Salas, in *Proceedings of the 13th International Pyrotechnics Seminar, Grand Junction, CO,* USA, 1988, p. 505.
4. R. G. Jungst and F. J. Salas, et al., in *Proceedings of the 15th International Pyrotechnics Semenar, Boulder, CO,* USA, 1990, p. 549.
5. A. V. Chernai, V. V. Sobolev, V. A. Chernai, et al., Combust., Explos., Shock Waves **39** (3), 335 (2003).
6. A. A. Brish, I. A. Galeev, B. N. Zaitsev, E. A. Sbitnev, and L. V. Tatarintsev, Combust., Explos., Shock Waves **5**, 326 (1969).
7. I. A. Galeev and B. N. Zaitsev, Combust., Explos., Shock Waves **5**, 447 (1969).
8. V. B. Ioffe, A. V. Dolgolaptev, V. E. Aleksandrov, and A. P. Obraztsov, Combust., Explos., Shock Waves **21** (3), 316 (1985).
9. B. P. Aduev, D. R. Nurmukhametov, R. I. Furega, A. A. Zvekov, and A. V. Kalenskii, Russ. J. Phys. Chem. B **7**, 453 (2013).
10. A. V. Kalenskii, A. A. Zvekov, M. V. Anan'eva, I. Yu. Zykov, V. G. Kriger, and B. P. Aduev, Combust. Explos., Shock Waves **50**, 333 (2014).
11. A. V. Kalenskii, M. V. Anan'eva, A. A. Zvekov, and I. Yu. Zykov, Tech. Phys. **60**, 437 (2015).
12. V. I. Tarzhanov, A. D. Zinchenko, V. I. Sdobnov, et al., Combust., Explos., Shock Waves **32** (4), 454 (1996).
13. B. P. Aduev, D. R. Nurmukhametov, G. M. Belokurov, A. A. Zvekov, A. V. Kalenskii, A. P. Nikitin, and I. Yu. Liskov, Tech. Phys. **59**, 1387 (2014).
14. A. A. Zvekov, A. V. Kalenskii, A. P. Nikitin, and B. P. Aduev, Comp. Opt. **38**, 749 (2014).
15. A. A. Zvekov, A. V. Kalenskii, B. P. Aduev, and M. V. Anan'eva, J. Appl. Spectrosc. **82**, 213 (2015).
16. A. V. Kalenskii, A. A. Zvekov, A. P. Nikitin, M. V. Anan'eva, and B. P. Aduev, Opt. Spectrosc. **118**, 978 (2015).
17. V. G. Kriger, A. V. Kalenskii, A. A. Zvekov, I. Yu. Zykov, and B. P. Aduev, Combust. Explos., Shock Waves **48**, 705 (2012).
18. B. P. Aduev, M. V. Anan'eva, A. A. Zvekov, A. V. Kalenskii, V. G. Kriger, and A. P. Nikitin, Combust. Explos., Shock Waves **50**, 704 (2014).
19. E. I. Aleksandrov and V. P. Tsipilev, Combust., Explos., Shock Waves **20** (6), 690 (1984).
20. V. M. Lisitsin, V. P. Tsipilev, G. Damamme, and D. Malis, Combust. Explos., Shock Waves **47**, 591 (2011).
21. V. G. Kriger, A. V. Kalenskii, and A. A. Zvekov, Combust. Explos., Shock Waves **46**, 60 (2010).
22. V. G. Kriger, A. V. Kalenskii, A. A. Zvekov, A. P. Borovikova, and E. A. Grishaeva, Combust. Explos., Shock Waves **48**, 488 (2012).

23. V. P. Tsipilev, Izv. TPU **306** (4), 99 (2003).
24. Yu. A. Zakharov, V. M. Pugachev, A. N. Popova, et al., Bull. Russ. Acad. Sci.: Phys. **77**, 142 (2013).
25. V. G. Kriger, A. V. Kalenskii, M. V. Anan'eva, and A. P. Borovikova, Combust. Explos., Shock Waves **44**, 190 (2008).
26. E. D. Aluker, A. S. Zverev, A. G. Krechetov, A. Yu. Mitrofanov, A. O. Terentyeva, and A. V. Tupitsyn, Russ. J. Phys. Chem. B **8**, 687 (2014).
27. V. G. Kriger, V. P. Tsipilev, A. V. Kalenskii, and A. A. Zvekov, Combust. Explos., Shock Waves **45**, 729 (2009).
28. E. T. Denisov, *Liquid-Phase Reaction Rate Constants* (IFI/Plenum, N.Y., 1974).
29. V. M. Zolotarev, V. N. Morozov, and E. V. Smirnov, *Optical Constants of Natural and Technical Media* (Khimiya, Leningrad, 1984) [in Russian].
30. V. G. Kriger, A. V. Kalenskii, I. Yu. Zykov, I. Yu. Zykov, and A. P. Nikitin, Thermophys. Aeromech. **20**, 367 (2013).
31. S. Vyazovkin and Ch. A. Wight, Thermochim. Acta **340–341**, 53 (1999).
32. E. T. Denisov, *Kinetics of Homogeneous Chemical Reactions* (Vyssh. Shkola, Moscow, 1988) [in Russian].
33. P. J. Robinson and K. A. Holbrook, *Unimolecular Reactions* (Wiley, London, 1972).

Translated by D. Zvukov